AIAA JOURNAL
Vol. 49, No. 3, March 2011

Flow Control Techniques for Transport Aircraft

Arvin Shmilovich* and Yoram Yadlin†
The Boeing Company, Huntington Beach, California 92647

DOI: 10.2514/1.J050400

A set of flow control approaches have been recently investigated for improved aerodynamic performance in a range of transport aircraft applications. Active flow control concepts are employed for improving airplane takeoff and landing performance, reducing operational hazards during airplane ground maneuvering, and alleviating trailing wakes for higher air traffic efficiency. Computational fluid dynamics has been used to gain insight into complex flows subject to various modes of actuation and to develop promising techniques of flow control. The use of numerical simulations is especially important in scenarios involving powered systems, intricate vortex structures, separated flows, and active flow control devices, for which alternative testing is extremely expensive and often impractical. This study represents an essential element in The Boeing Company's approach to development of flight-worthy integrated active flow control systems.

Nomenclature

α	=	angle of attack
C_L	=	lift coefficient
$C_{L\,\max}$	=	maximum lift coefficient
C_{mac}	=	wing mean aerodynamic chord
C_μ	=	slot momentum coefficient, $(h/c) \cdot (\rho_j/\rho_\infty) \cdot (U_j/U_\infty)^2$
c	=	chord length
F^+	=	reduced forcing frequency, $f \cdot c/U_\infty$
f	=	actuator frequency, Hz
h	=	actuator slot width
M_∞	=	freestream Mach number
P_T	=	total pressure
P_{T_∞}	=	freestream total pressure
R_N	=	Reynolds number
rad	=	vertical coordinate passing through vortex center
U_j	=	peak jet velocity
U_θ	=	crossflow velocity
U_∞	=	freestream velocity
u_x	=	streamwise component of velocity
δ_{flap}	=	flap deflection angle
ρ_j	=	jet actuator density
ρ_∞	=	freestream density

I. Introduction

IN RECENT years a variety of flow control techniques have been developed for a wide range of applications [1–5]. Reduced flow separation is an example of a targeted application in which significant breakthroughs have been achieved using active flow control (AFC) for improved aerodynamic performance. A review of flow control applications for several body shapes and simple airfoils is given by Wygnanski [2]. Several studies were geared toward demonstrating the effectiveness of pulsed actuation in controlling the leading-edge flow separation, which occurs for airfoils at high angles of attack. Other examples include airfoil sections with relatively simplified high-lift devices: i.e., drooped leading edges and simple-hinge flap elements. Although significant inroads have been made in the context of relatively simple airfoil shapes, the question of whether AFC could be integrated into a practical airplane design is still outstanding. This is crucial, since one of the principal design objectives of commercial and military airplanes is to achieve mission requirements for takeoff and landing. Because superior high-lift capability is a key objective, it is important to assess the merit of AFC and to establish performance increments. The current study is aimed at identifying potential implementations of flow control for a set of high-lift wing sections and providing guidelines on practical modes of actuation.

Potential extensions of AFC for control of vortex systems to enhance airplane operational capabilities are also explored. One application addresses the engine ingestion of ground vortices that occurs at certain conditions around airplanes operating in ground proximity. Engine vortex ingestion poses a serious operational hazard, due to the risk of foreign-object damage (FOD) and engine surge. Another application of AFC is aimed at control of trailing wakes. The flow control objective is to permit safer and shorter airplane separation distances, thereby mitigating airport congestion. In the context of improved rotorcraft efficiency AFC techniques are sought to reduce blade–vortex interaction to suppress noise from the blades.

This study addresses the development of a set of flow control approaches for the respective aerodynamic flow problems. It underscores the importance of numerical simulation in identifying candidate flow control approaches and effective modes of actuation. The computational method was validated for sets of experimental data obtained for several high-lift systems. This included a range of Reynolds numbers up to representative flight conditions. The validity of the numerical method has firmly placed computational analyses as a core element of The Boeing Company's strategy for AFC development. The use of numerical simulations is extremely important in situations involving powered systems, complex vortex structures, separated flows, and active flow control devices, for which alternative testing is extremely expensive and often impractical. This is particularly critical in the context of the current AFC applications.

In this paper the numerical tool will be reviewed in the context of time-dependent modeling for a set of actuation patterns. Validation of the computational procedure with experimental data for the respective applications will be presented. The aerodynamic problems will be described, and potential solutions based on AFC will be investigated. Various diagnostics tools will be employed to identify promising AFC implementations for the set of aerodynamic problems.

II. Numerical Procedure

The numerical tool used for the simulation of active flow control is a modified version of the OVERFLOW code originally developed by

Presented at the ICAS 2008 Congress, Anchorage, AK, 14–19 September 2008; received 17 March 2010; revision received 18 August 2010; accepted for publication 28 October 2010.

*Boeing Technical Fellow, Platform Performance Technologies, Boeing Research and Technology, 5301 Bolsa Avenue, Mail Stop H45N-E405. Senior Member AIAA.

†Senior Engineer/Scientist, Platform Performance Technologies, Boeing Research and Technology, 5301 Bolsa Avenue, Mail Stop H45N-E405. Senior Member AIAA.

NASA [6]. OVERFLOW uses the unsteady Reynolds-averaged Navier–Stokes formulation for overset grid systems. The numerical procedure has been modified to facilitate the development of a family of flow control techniques for vortex alleviation and reduced flow separation. Special modules have been developed for the modeling of time-varying boundary conditions to simulate flow excitation due to control devices. Jet actuation is described by the mass flow rate, cross-sectional area, stagnation pressure, and temperature to define the velocity at the ejection nozzle. The numerical algorithm uses the characteristics approach for consistent application of the boundary conditions.

The current flow control techniques can be generally grouped in two basic actuation modes. One group employs pulsed actuation, which is used to model synthetic jets and non-zero-mass-flow actuation. In the case of pulsed jets, the flux vector is aligned with the nozzle axis and jet pulsation is determined by the forcing frequency. Various signal shapes ranging from sinusoidal to step function (i.e., jet velocity as a function of time) are defined by sets of analytical functions with continuous first and second derivatives.

The second family of flow control actuators is based on periodic motion of the ejection nozzle, much like a water sprinkler system. Jet flow is continuous, but the fluid is discharged through a swiveling nozzle. A direct approach for modeling jet ejection from moving nozzles requires moving-grid systems. To avoid this complexity and to simplify the computational procedure, two alternative implementations of boundary conditions were employed to approximate moving jets. In one implementation the nozzle is assumed to be stationary, but the jet flux vector at the exit plane is prescribed in a time-varying fashion to mimic the swiveling motion of the nozzle. For a fixed jet velocity at the nozzle exit this treatment produces a nonconstant jet mass flow rate as the jet vector cycles through. In an alternative version that preserves constant jet mass flow, the jet velocity is periodically modified according to the instantaneous angle between the jet vector and the nozzle exit plane. Further details on the boundary conditions are described in [7,8]. The current study indicates that the two optional sets of boundary conditions produce similar global flows, although the time-varying flow characteristics are slightly different. The constant-mass-flow condition is used in the simulations presented here.

The calculations were obtained using a second-order upwind-differencing scheme. Depending on the application, either the Spalart–Allmaras (SA) or the shear stress transport (SST) turbulence models have been used. The flow control computations use a second-order time-accurate scheme. Time dependent simulations are initiated from a steady-state solution obtained for the flow in the absence of any actuation. A minimum of 800 time steps per actuation cycle are used, depending on the application and frequency of actuation. Time-step requirements for evaluating the effects due to actuation frequency will be further discussed in the context of the wing vortex problem.

III. Enhanced High Lift for Takeoff and Landing

Takeoff and landing performance are two of the principal design objectives of transport airplanes. Whether the requirement is for a higher airplane weight or for shorter runways, superior high-lift capability is a key requirement of the airplane manufacturers. Techniques for altering the viscous flow structures at high-lift conditions are highly desirable, due to the potential for improved efficiency. Although previous investigations of AFC demonstrate various degrees of performance improvements, it is not clear that the gains are substantial enough to warrant the development of a whole new airplane based on this technology. It is therefore important to explore ways of AFC implementation for providing very high performance levels while addressing issues of practical airframe integration. In the application of AFC to high lift the numerical tool was first validated against experimental data for several wing sections and various actuation modes. Numerical simulations were then used to develop flow control approaches for a set of high-lift systems.

A. Numerical Simulations

The numerical implementation and validation for several wing sections are described in [9,10]. Results for two wing sections will be presented here. Both the SA and SST turbulence models have been used, producing very similar results. The SA turbulence model was used for obtaining the results described here. The first wing section was tested by Kiedaisch et al. [11], and it consists of simple-hinge leading-edge and flap elements. The model was mounted between two walls, and the objective was to obtain 2-D flow characteristics. Two-dimensional flow simulations for airfoil sections in free air were used in this study. In the computational model the actuator is represented by a nozzle having a constant-cross-sectional area, and it is embedded within the airfoil at the flap hinge line. The nozzle area and its orientation are consistent with the area and angle of the actuator at the exit station in the experimental setup.

Validation is presented for a 15° leading-edge droop and a flap deflection of 40°. A freestream having a Mach number of 0.09 and a chord Reynolds number of 0.75×10^6 were used. First, a steady-state solution was obtained for the baseline flow without actuation. Actuation was then applied in the form of a sinusoidal signal with a

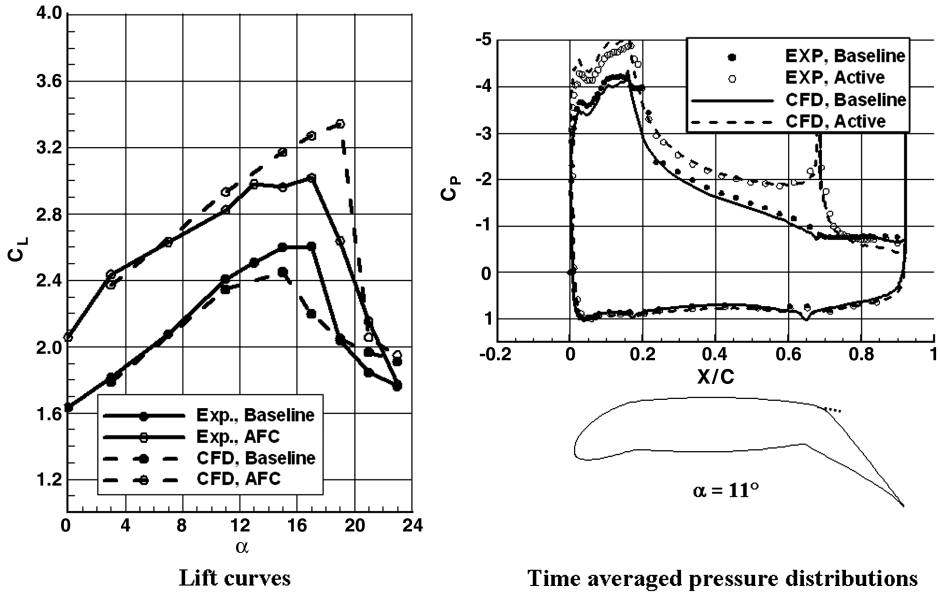

Lift curves **Time averaged pressure distributions**

Fig. 1 Validation for the simple-hinge high-lift configuration ($M_\infty = 0.09$ and $R_N = 0.75 \times 10^6$).

frequency of 217 Hz ($F^+ = 2.56$) and momentum coefficient C_μ of 0.015, corresponding to jet maximum velocity of about 2.5 times the freestream velocity. Limit-cycle convergence was obtained after approximately 40 actuation cycles.

Figure 1 shows comparison with experimental data in terms of time-averaged lift and pressure distributions, demonstrating the benefit of AFC. Good agreement is obtained in the linear range of angles of attack for both the baseline and the flow-actuated cases. However, major discrepancies exist at the $C_{L\max}$ conditions. There are quite a few sources of inconsistencies, which might explain the poor agreement at high flow incidence. From the experimental standpoint, since there was no sidewall boundary-layer treatment, the separation pattern at large incidence was most likely contaminated by the separation of the viscous layers of the sidewalls. This effect is particularly detrimental for the small span-to-chord ratio of 1.57 in this experiment. With respect to the flow analysis, the computational tool is not accurate at $C_{L\max}$ conditions, due to shortcomings in turbulence modeling. Another source of inconsistency is the AFC application, where the actuation signal prescribed in the simulations is not identical with the experiment. In view of all the uncertainties, the computational predictions are quite encouraging, especially in the linear range. Since lift augmentation due to AFC is reasonably well captured, the analysis tool has been used for developing more practical AFC implementations with higher aerodynamic efficiency.

The agreement between the numerical predictions and low-Reynolds-number experimental data in terms of time-averaged forces and surface pressure distributions has given confidence in using computational fluid dynamic (CFD) for other AFC implementations. In a follow-up study the numerical technique was used to guide the high-Reynolds-number design of a multi-element configuration representing an airplane transport. It consists of a drooped leading edge and a slotted flap. Wind-tunnel experiments were subsequently performed at the NASA Langley Research Center's low-turbulence pressure tunnel at representative full-scale Reynolds numbers. Flow measurements were obtained for sets of port layouts and actuation modes. The experimental data was then used to validate the CFD tool. Comparison between the experimental data and numerical predictions are shown in Fig. 2 for $M_\infty = 0.1$ and Reynolds number of 9×10^6. The actuation is applied at the flap close to its leading edge in the form of an asymmetrical wave with approximate step-function shape, consistent with the signal produced by the electromagnetic actuator used in the experiment. The agreement with the experimental data is satisfactory and the overall lift magnitudes are well predicted. Near $C_{L\max}$, relatively small differences exist between the predicted and measured maximum lift and stall angles. The validation step confirms that using the computational method to develop a flight representative high-lift system powered by AFC is a prudent approach. A more detailed description of validation with flow measurements obtained for various port layouts and actuation modes is given in [10].

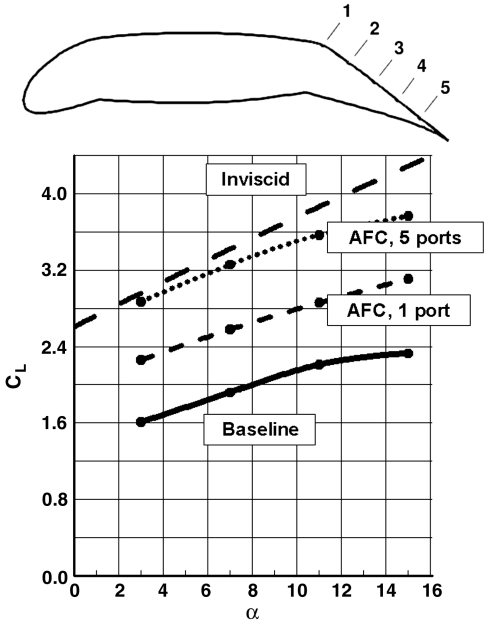

Fig. 3 Lift augmentation due to distributed flow control: simple-hinge flap.

B. Single-Element Section

High-lift systems that consist of simple-hinge moveable elements are very attractive, since they are light and mechanically simpler than slotted multi-element systems, resulting in lower manufacturing cost. The aerodynamic characteristics of simple-hinge systems are not as good as slotted wing sections. The objective is to augment their performance using AFC. The single-element airfoil from the previous section is considered here. Results for a flap deflection of 25° are shown in Figs. 3 and 4. The freestream Mach number is 0.09 and chord Reynolds number is 0.75×10^6. The baseline flow consists of a very large flow-separation bubble at the flap, resulting in maximum lift of about 2.4. A sinusoidal signal similar to that used in the validation step ($C_\mu = 0.015$ and $f = 217$ Hz) is first applied at the hinge line where the separation originates in the baseline case. The computations indicate that AFC is effective, providing a lift increment of approximately 0.65 in the linear lift range. In a time-average sense the application of AFC at the hinge line is only partially effective, reducing flow separation in the front portion of the flap. For reference, results of the inviscid simulations are also shown in the figures. Inviscid lift determines the theoretical upper limit of an airfoil to produce lift in the absence of viscous effects and is conveniently used as a yardstick for AFC efficiency.

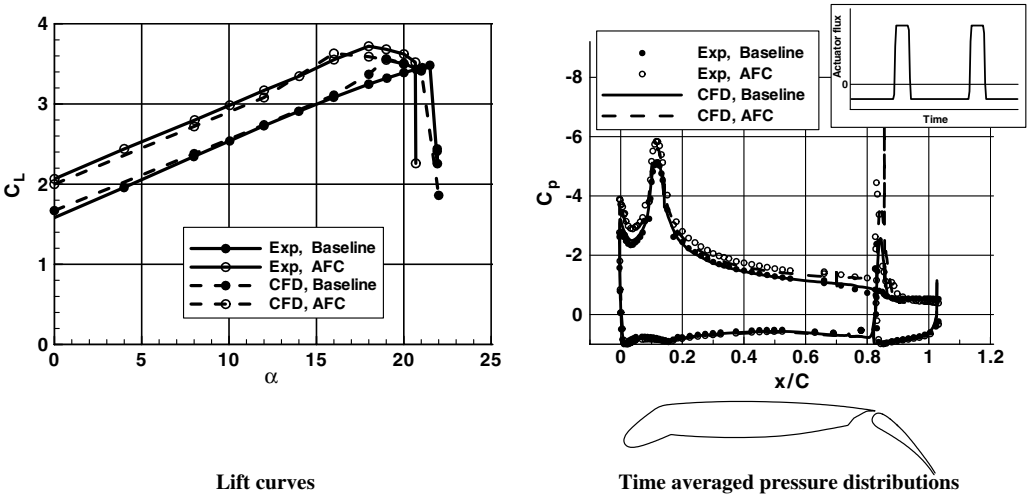

Lift curves **Time averaged pressure distributions**

Fig. 2 Validation for the multi-element configuration ($M_\infty = 0.10$ and $R_N = 9 \times 10^6$).

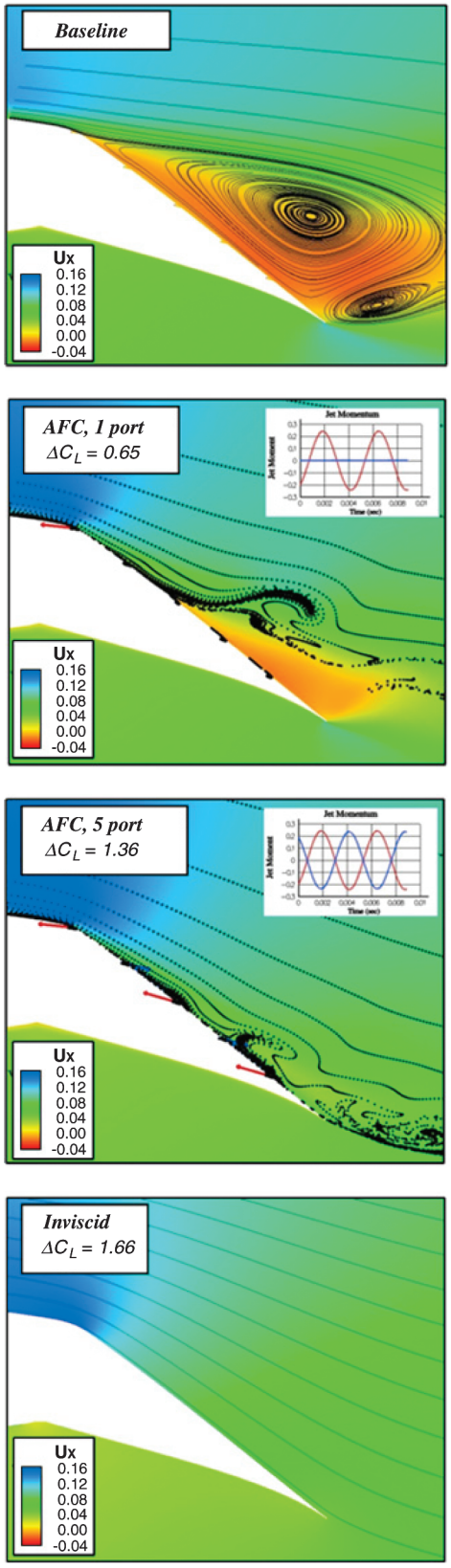

Fig. 4 Instantaneous flowfield description for a simple-hinge flap system (streamwise component of velocity, $\alpha = 11°$).

Simultaneous actuation is then applied at five ports along the flap. The actuation parameters applied at each port are similar to the single-port actuation described earlier. A phase shift of 180° between adjacent ports is used. A unique flow structure ensues in this case, where the original separation bubble is effectively altered to a predominantly attached flow. The cumulative effect provided by the multiple ports results in a lift gain of 1.33 relative to the baseline, and it represents more than twice the gain realized with the single port. Further confirmation of the effectiveness of distributed actuation is demonstrated by the resemblance of this flow control mode with the inviscid case in Fig. 4. The lift is also close to the level obtained in the inviscid case.

C. Multi-Element Wing Sections

The next set of simulations focuses on AFC for multi-element systems, where the flow is highly interactive. For instance, the trailing-edge flap is strongly influenced by the downwash generated by the lift on the main wing. Several factors can limit the maximum lift that can be achieved by a multi-element system. The maximum lift is limited by viscous effects due to the very strong pressure gradients introduced by the high suction levels. Or it can be limited by boundary-layer separation in the vicinity of the slat and main wing leading edge. It can also be limited by boundary-layer thickening or separation on the trailing edge of the main wing or on the flap elements. Another limitation can occur due to bursting of the viscous wake from the slat or the main wing as it passes through the high-pressure gradients developed by the flap. In this case, the boundary layers on each of the high-lift components may be attached, but the rapid spreading of the viscous wakes will limit the maximum lift that can be achieved [12]. An attempt to improve the flow over a high-lift system by addressing one of these limiting factors may improve the performance, but it will still be limited by the other factors. The goal is to identify AFC implementations with meaningful performance improvements by addressing all of these effects. This will be evaluated for configurations that are optimized for high lift.

1. *Conventional Wing Section*

The conventional airfoil represents a typical transport, and it is derived from the wing of the McDonnell Douglas MD80 airplane. This high-lift system employs a flap with moderate Fowler motion. The effect of distributed AFC at a representative takeoff condition with flap deflection of 24° is shown in Figs. 5 and 6. Sinusoidal pulsation of 20 Hz ($F^+ = 1.52$) and momentum coefficient C_μ of 0.015 are applied at all ports. Out-of-phase actuation is applied at adjacent ports. The freestream Mach number is 0.1 and the chord Reynolds number is 3×10^6. The simulation indicates that at $\alpha = 19°$ the baseline flow is on the verge of separation at the trailing edge of the slat and in the aft portion of the main element. The combined 10-port actuation at the slat, wing, and flap elements according to the AFC layout described in Fig. 5 produces near-inviscid lift in the

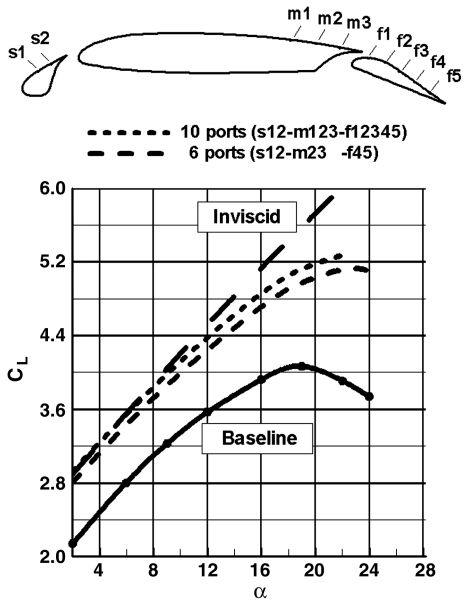

Fig. 5 Effect of AFC application at each element of the conventional high-lift wing section (representative takeoff configuration, $\delta_{\text{flap}} = 24°$).

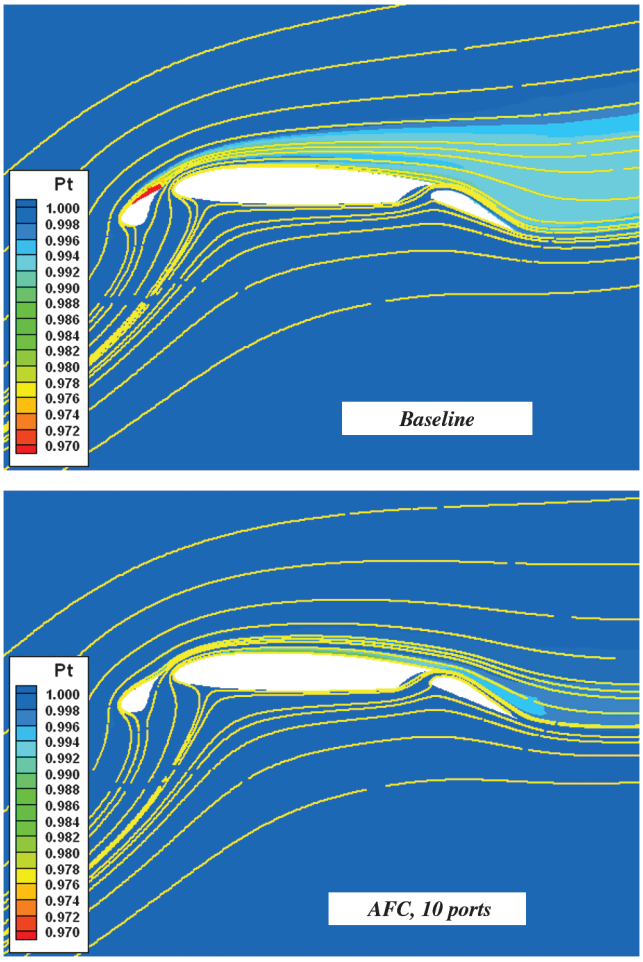

Fig. 6 Impact of AFC on flow structure of the conventional high-lift system (time-averaged total-pressure, $\alpha = 19°$).

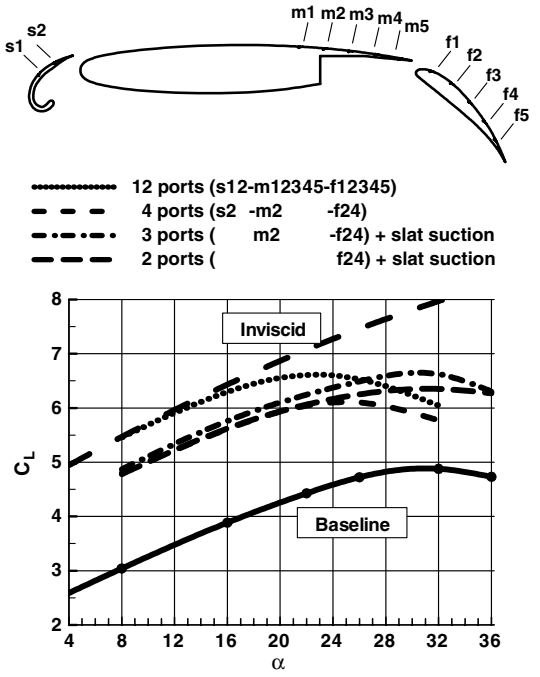

Fig. 7 AFC for advanced wing section (landing configuration, $\delta_{flap} = 50°$).

linear range and profound improvement in stall characteristics. The application of AFC at all wing elements is beneficial over the range of angles of attack. In particular, the actuation at the slat reduces the size of its wake considerably. Consequently, the slat wake traverses the adverse pressure-gradient regions of the main element and flap without significant degradation in flow quality. This results in less tendency for offsurface flow reversal, streamlined flow around the flap, and higher circulation. The streamlining effect is significant, resulting in a larger turning angle in the aft airfoil portion. For practical implementations it is also important to explore ways of minimizing the required input to the flowfield while still achieving meaningful lift increments. Results obtained for a six-port flow control pattern with two ports on each wing element are included in Fig. 5. Compared with the full AFC actuation, the six-port set results in relatively small degradation in lift.

2. *Advanced Wing Section*

The advanced wing section is derived from an experimental model that has been thoroughly tested and optimized for very high lift [13]. It consists of a variable-camber Krueger slat and a flap with extensive Fowler motion. Results for a 50° flap deflection are presented in Figs. 7 and 8. This is representative of landing conditions in which the baseline flow is separated over most of the flap, even at low angles of attack. The freestream conditions and actuation parameters are similar to those used in the conventional-wing-section case. The combined 12-port actuation results in smooth and attached flow on the upper surfaces of all elements. The circulation increases on all elements, as indicated by the counterclockwise movement of the stagnation points. Consequently, inviscid lift level is achieved in the linear lift range. The flow control at the slat boosts performance at

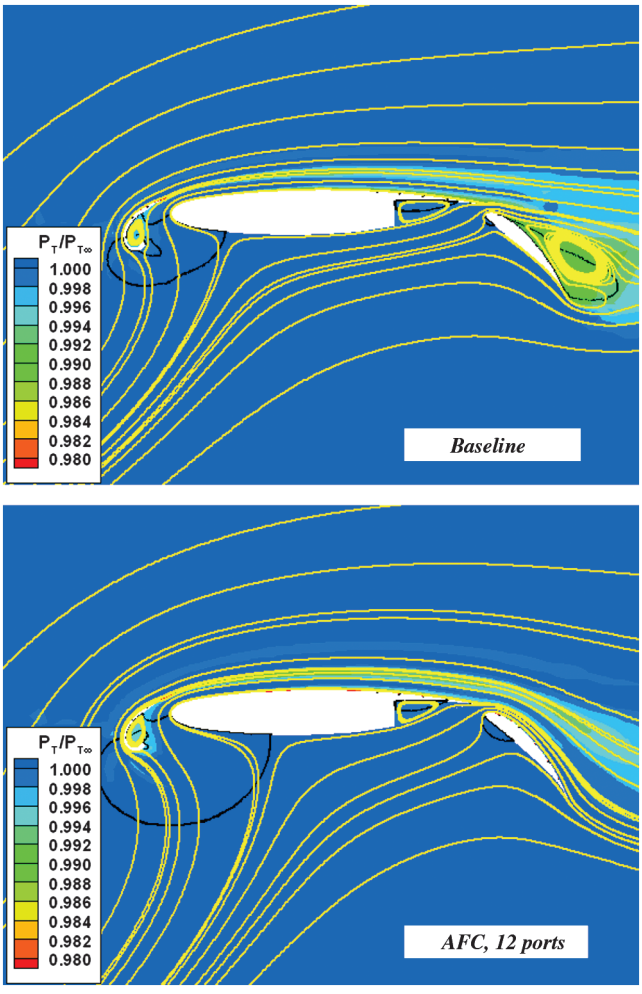

Fig. 8 Time-averaged total-pressure field showing impact of AFC on confluent viscous layers of the advanced wing section ($\alpha = 22°$). Black lines denote pockets of flow reversal.

high angles of attack by producing a wake that favorably interacts with the flow on the flap.

A four-port set has also been investigated, in which one port is employed at each of the slat and main elements and two ports are employed at the flap. This actuation mode reduces the lift in the linear range to about 70% of the level obtained with the full AFC application, with a commensurate drop in maximum lift.

The next set of flow control patterns includes constant suction at the slat in conjunction with zero-mass-flow actuation on the main element and the flap. The suction intensity is defined using a mass flow rate equivalent to the uniform flow, with a velocity equal to the maximum velocity of the pulsed jets. The results obtained with the AFC patterns employing suction are also shown in Fig. 7. The suction at the slat removes a portion of the bounded viscous layer, rendering a smaller trailing wake. The slat wake influences the flow over the flap and helps improve $C_{L\max}$. In particular, the m2-f24 pattern with slat suction produces maximum lift equivalent to that obtained with the 12-port actuation. A more detailed description of AFC for multi-element systems can be found in [14].

The purpose of the high-lift applications was to provide insight into AFC flow mechanisms and to establish guidelines for port placement. The exercises in which fewer ports are used (Figs. 5 and 7) demonstrate that it is possible to achieve meaningful lift increments using smaller AFC inputs. In this study there was no attempt to optimize AFC implementation for a given lift level. It is plausible that even smaller inputs to the flowfield could be achieved by regulating the jet intensity, frequency, and signal phase at individual ports.

IV. Alleviation of Engine Ground Vortex

Aircraft with turbojet engines mounted relatively close to the ground develop vortex activity during high-power, low-speed, and static ground operation. The suction generated by the engine results in the formation of a vortex on the ground. Usually, the ambient flow contains significant amounts of vorticity (turbulence) due to gusts, ground turbulence, wake flow of neighboring aircraft components (i.e., wing, fuselage), and mixing of engine reverser plumes when thrust reversers are deployed. The mechanism of ground vortex formation is the amplification of the seed vorticity in the ambient flow, due to the contracting streamlines approaching the inlet. This interaction results in a concentrated vortex originating at the ground plane and terminating inside the engine. The rotational flowfield induced by the ground vortex is the cause for kicked up dust and dirt, which can become entrained in the airflow drawn into the engine inlet. The tornadolike flow is capable of dislodging sizable foreign objects off the ground (for example, rocks, chunks of ice, or asphalt), causing FOD that may lead to engine failure. The vexing problem of ground vortex ingestion hinders the ability to land in austere fields and to perform essential ground maneuvers on unimproved terrain. Furthermore, the engine ingestion problem is exacerbated by the advent of larger and more powerful high-bypass turbojet engines.

One of the salient features of flows with increased propensity to ground vortex activity is the unsteady characteristic of the air motion. Flow visualization in full-scale experiments indicates that the flowfield is highly unsteady and the movement of the vortex origination point on the ground is sporadic. Consequently, the vortex filament fluctuates incessantly over a significant portion of the lower inlet sector. The apparent randomness of the flow in realistic and uncontrolled environments is due to gusts with varying strengths and direction (time variation of ambient flow), ensuing structural response of aircraft components (i.e., the flexing of the entire wing/engine assembly), and unsteady turbulent mixing of the thrust-reverser plumes.

There have been several attempts to solve the engine vortex ingestion, but none have proven to be satisfactory in an operational sense. Johns [15] reviewed these approaches from a practical point. Prior techniques target specific flow situations and do not provide effective solutions for real-life applications. Specifically, they constitute point-design solutions, since they provide localized treatment of a ground vortex without consideration of the inherent problem of sporadic vortex motion.

A couple of vortex disruption methods that address the unsteady characteristics of realistic inlet vortex flows have been recently developed. The pulsed-jet device developed by Smith and Dorris [16] uses high-pressure air to alternatively eject fluid from two nozzles mounted underneath the engine nacelle close to the nacelle lips. The intermittent high-frequency ejection provides turbulent mixing to prevent the formation of a coherent vortex. The sprinkler jet actuator proposed by Shmilovich et al. [17] uses continuous ejection through a moving nozzle mounted on the nacelle lip to provide wide-area coverage, thereby reducing the risk of vortex ingestion, even when the vortex moves rapidly. The effectiveness of these inlet vortex-alleviation methods has been demonstrated for isolated engines in proximity to the ground plane [7]. More specifically, the simulated flowfields obtained with the pulsed-jet actuation are consistent with the experimental observations in a laboratory experiment reported in [18]. The current analyses focus on the evaluation of the control systems for full airplane configurations.

A. Simulations of Airplane Vortical Flows

The development, analysis, and testing of vortex-alleviation devices are daunting tasks. Engine integration issues have been traditionally addressed by employing cut-and-try approaches or knowledge-based engineering obtained from relatively simple experiments. Unfortunately, testing in a controlled laboratory setting does not represent realistic operational conditions. Consequently, these design approaches have sometimes led to unsatisfactory solutions. Compounding the problem are the complexity and cost of testing with powered engines, thrust reversers, and actuation devices. In the case of full-scale testing there is a reluctance to subject the engines of the test airplane to the risk of costly repairs due to FOD or engine surge. Hence, there is a critical need for an efficient computational technique as a primary development tool.

The current numerical procedure has been applied to a realistic four-engine transport airplane operating on the ground with thrust reversers deployed [19]. The SST turbulence model was used. Validation was first done for a full-scale experiment. One of the difficulties with such experiments is that vortices are usually invisible and can be observed only when they contain dust particles or water droplets. If the humidity level in the prevailing flow is high, the vortices are rendered visible, due to condensation in the low-pressure regions of their cores. In this particular experiment the test airplane was positioned over a shallow pool of water, where the vortex elements can be detected by the droplets entrained into the flow. The ambient conditions in these tests cannot be controlled and tend to fluctuate. As a result, duplicating the exact test conditions in the numerical simulation is not trivial. However, it is possible to simulate the nominal wind conditions and compare the general characteristics of the flow. A comparison of numerical simulations with the full-scale operational airplane is presented in Fig. 9 for a tail wind of 10 kt, consistent with the measured ambient wind condition. The flow structure in the computed flowfield is described by streamlines colored by Mach number, where blue denotes very low velocity and red designates a Mach number of 0.8. The computed results indicate a vortex at a location similar to that observed in the experiment. Note that the thrust reversers' plumes, indicated by the streamlines in the computed cases, are not visible in the experiments.

Additional comparisons of the numerical simulations with observations of vortex flow structures around full-scale airplanes are presented in Fig. 10. Here, the ambient wind conditions are nearly static and the structure and the locations of the inlet ground vortex systems are very similar to the computed flowfields. In these simulations the flow structure is described by streamlines, with no physical significance to their color. It is interesting that even though the engines operate at similar power settings, ground vortices occur only at the inboard engines. This is due to the difference in the capture stream tubes of the various engines [19]. Note that for the airplane shown at the bottom of Fig. 10 the actual thrust-reverser plumes are

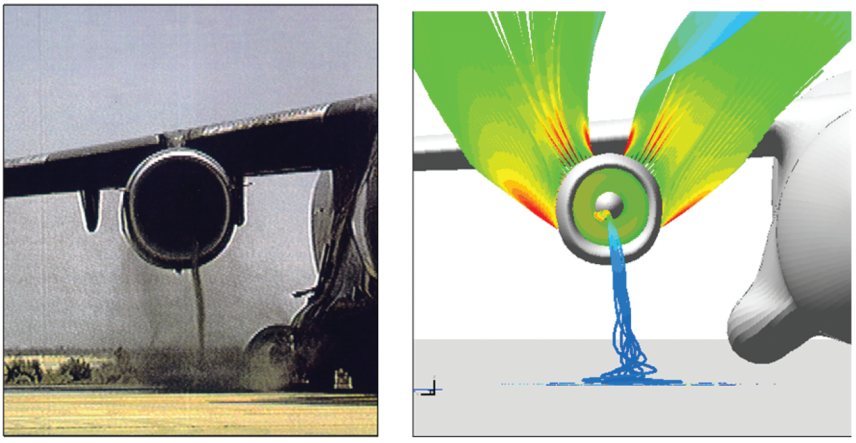

Observation Simulation

Fig. 9 Comparison of full-scale experiment with the numerical simulation (tail wind of 10 kt).

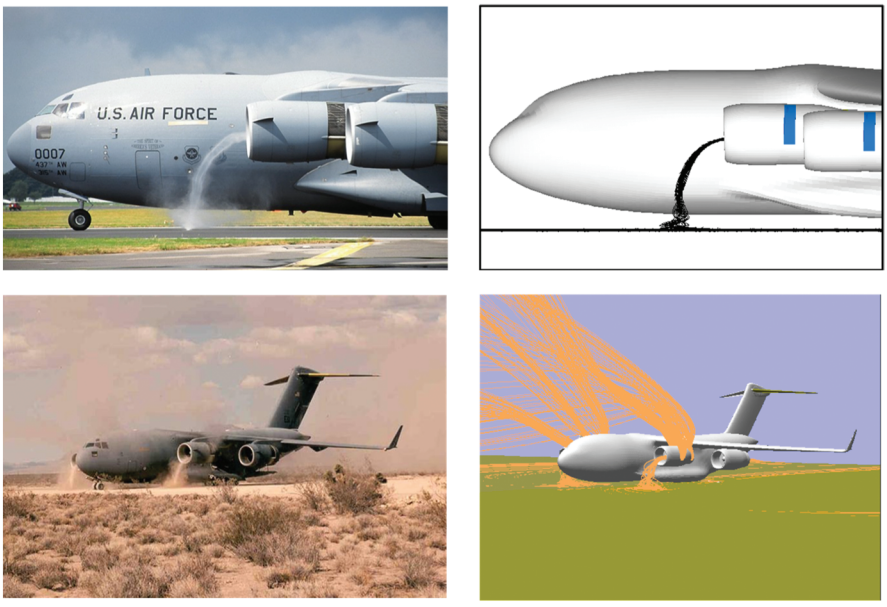

Observations Simulations

Fig. 10 Vortical systems around airplanes during ground operations and comparisons with numerical simulations.

visible, due to the dust particles ingested by the engines. Further details on the numerical implementation and insightful discussion on the flow structure around multi-engine airplanes in ground operation can be found in [19].

B. Methods of Vortex Control

The flow control techniques use fluidic injection in critical regions close to the engine inlet. The flow actuation is accomplished by high-pressure bleed air from the compressor, which is supplied to a valve located inside the engine cowl and close to the nacelle lip. The amount of air required to affect the inlet vortex is less than 1% of total inlet flow, which is well within the bleed limit of the engine. Two modes of actuation have been considered for the treatment of vortex ingestion.

1. Pulsed Actuation

The pulsed-jet system [16] uses high-pressure air to alternately eject fluid from two nozzles mounted underneath the engine nacelle close to the nacelle lips. This type of actuation can be obtained by fluidic valves that are used in various industrial applications. The nozzles would be deployed during low aircraft speed and high engine power setting. The injection nozzles are directed upstream and toward the ground plane. The intermittent high-frequency ejection provides sufficient turbulent mixing to avoid the formation of a coherent vortex.

The effect of pulsed actuation is demonstrated on a transport airplane that includes all relevant components for adequate representation during ground operations. Each actuation unit consists of a pair of nozzles and is included at each engine, as shown in Fig. 11. The nozzles are pointing 15° inward and 30° below the horizon. A tail

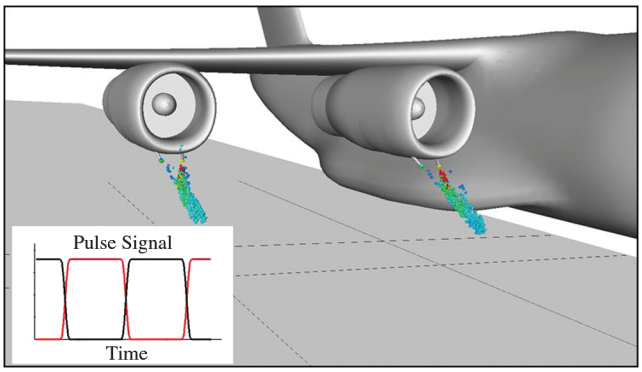

Fig. 11 Pulsed-jet ejection described by particles released from actuator nozzles. Particles are colored by Mach number (red is near sonic).

wind of $M_\infty = 0.007$ is considered in the simulation. A high power setting is used at each engine to simulate realistic operational conditions. The flow control signal consists of a pulsed jet at a frequency of 140 Hz, defined by a signal resembling a step function. This actuation frequency is within the practical range of 100–180 Hz provided by typical two-nozzle fluidic actuators [18]. Aspects of integration into realistic engines, combined with the guidelines in [16], led to the design of the nozzle layout. The inset describes the signals of each actuation unit. The short time scale of the ejection patterns is illustrated by releasing particles from the nozzles during the first five actuation cycles. The particles are colored by the local Mach number, where red represents high velocity. In this snapshot one nozzle blows at maximum velocity, close to sonic, and the other nozzle has zero jet velocity.

The global flow structure is described in a series of snapshots in Fig. 12, where the actuation starts at $t = 0$. Traces of particles released at select locations on the ground plane and on the fuselage are used to examine the vortex system in the transient flowfield. The ground plane is described by the pressure field. In the baseline flow ($t < 0$) the outboard engine is largely exposed to the oncoming tail wind, and therefore it does not develop a vortex off the ground plane. In contrast, the inboard engine experiences flow blockage due to the fuselage and the outboard engine, resulting in high suction power to satisfy the inlet airflow requirement. The suction results in the formation of the ground vortex, leading to inboard engine ingestion. Moreover, due to the proximity of the inboard engine to the fuselage,

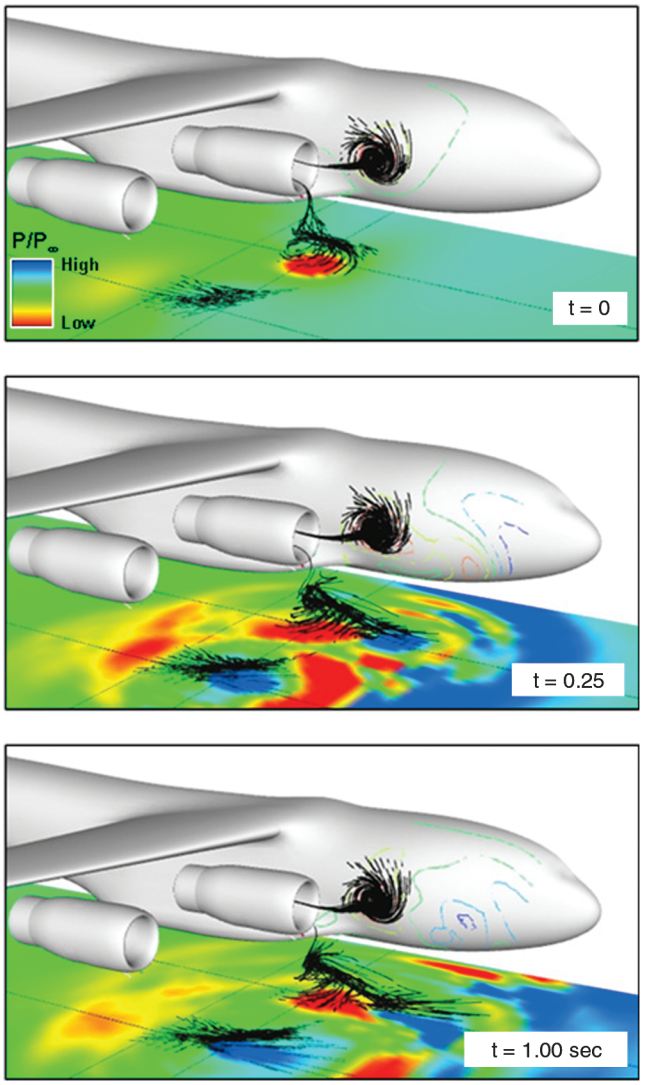

Fig. 12 Flow development due to pulsed-jet actuation (pressure contours on the ground plane and particle traces originating from the ground plane and fuselage).

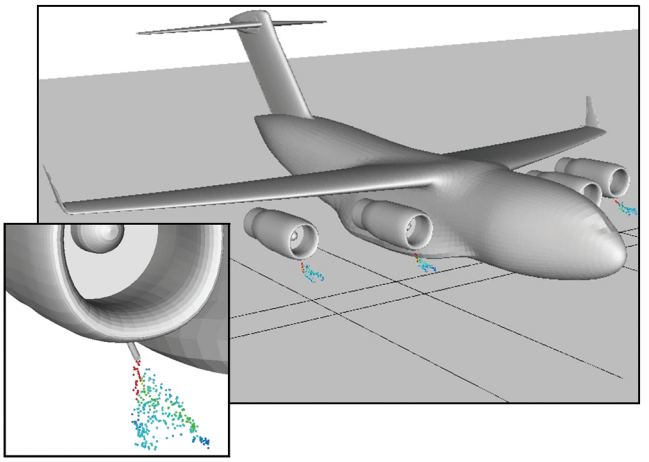

Fig. 13 Sprinkler jet ejection described by particles released during the first five cycles (0.036 sec) from start of actuation. Particles are colored by Mach number (red is near sonic).

an additional vortex element is formed off the fuselage surface. The fuselage vortex is also ingested by the inboard engine, but it does not pose a risk of FOD. A more thorough description of the vortical structure around airplanes in ground operations is given in [19]. The excitations introduced by the jets affect the flow in front of the engines. The pressure waves created by the periodic jets impinge on the ground and disperse in a radial direction in the region underneath the engines. According to the simulation, as time progresses, the

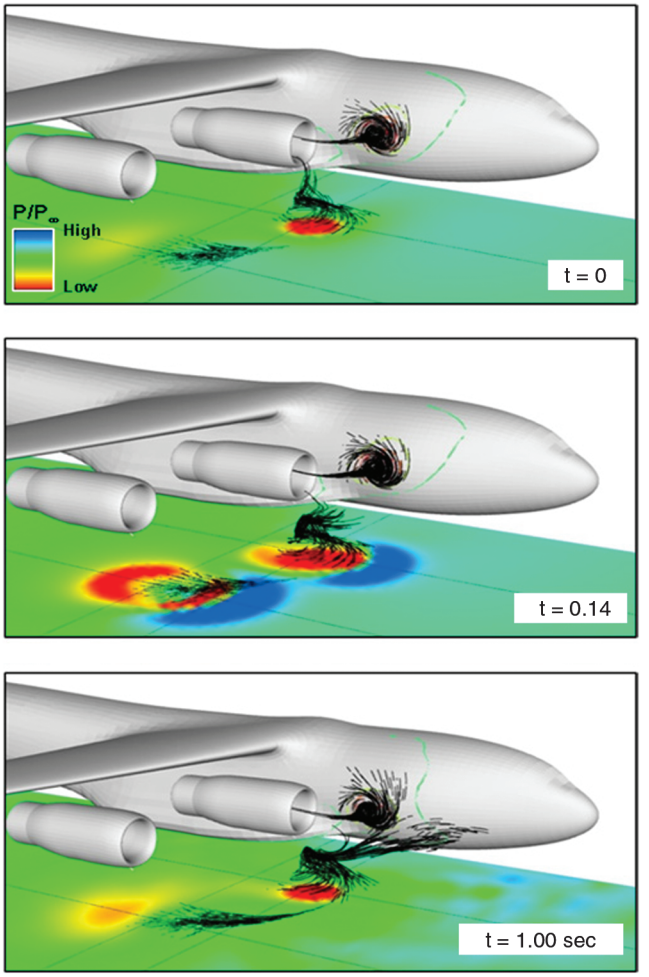

Fig. 14 Flow development due to sprinkler actuation (pressure contours on the ground plane and particle traces originating from the ground plane and fuselage).

vortex filament is pushed away from the engine in the forward direction, toward the front of the airplane. Note that the vortex originating at the side of the fuselage is hardly affected by the actuation.

2. Sprinkler Actuation

The sprinkler system uses a single nozzle located close to the nacelle lip [17]. During actuation the nozzle swivels according to a prescribed motion to inject flow into a large domain in front of the engine inlet in the general upstream direction. The slew motion of the ejecting fluid disrupts the global flowfield in front of the engine and prevents the formation of vortices. Since realistic full-scale engine vortex ingestion is a highly unsteady phenomenon, with the vortex meandering underneath the engine, this method is very effective in breaking up of the nonstationary ground vortex.

Wind conditions and engine power setting as in the pulsed-jet case are used for the sprinkler actuation. The sprinkler jet actuation is applied at the lower part of each engine, close to the inlet lips. The nozzle is pointed at an angle of 20° below the horizontal plane, and the jet moves side to side within a $\pm 30°$ range at a frequency of 140 Hz. The short-time-scale flow development in the vicinity of the engine highlight regions is presented in Fig. 13, where particles are released from the nozzles during five cycles from start of actuation.

The long-time-scale flow development is examined in Fig. 14. The intermittent motion provided by the periodic excitation at the bottom side of each of the engine cowls perturbs the flow in front of the engines. After 0.14 s the perturbations reach the ground surface, and pressure waves are generated in the near field underneath the respective engines. The ripple effects propagate radially with decreasing intensity in pressure fluctuations until the flow reaches a limit-cycle behavior at $t > 1.00$ s. The ground vortex is disrupted close to the inboard engine inlet at $t = 0.14$ s. The subsequent time frames show that the vortex filament is altered by the ejecting flow and it is expelled away from the engine. Engine vortex ingestion from the bottom side has been curbed by the sprinkler actuation, whereas the vortex off the fuselage is only slightly affected.

V. Wing Wake Alleviation

An area of high priority in the aerospace transport industry is solving the looming problem of airport congestion. The capacity of many airports is close to saturation, yet the number of aircraft in commercial aviation is projected to double in the next 12 years. Current airport capacity is largely controlled by the frequency with which planes can be brought in and out of the airport. A pacing item in landing and takeoff frequency is the time necessary for the dissipation of wake vortices produced by planes in motion, since trailing vortices pose particularly dangerous conditions for following airplanes. The eventual breakup of the vortices is the result of instabilities generated by perturbations due to ambient turbulence [20]. Unfortunately, these instabilities evolve very slowly and do not result in flow conditions that allow meaningful reductions in airplane separation. Trailing vortices have caused numerous airplane crashes and have been a main concern for the Federal Aviation Administration and similar organizations around the world. Currently, the only way to solve the problem of this invisible hazard is to avoid the flight path of large aircraft. Air traffic regulations require aircraft separation to be maintained to ensure that severe vortex encounters are avoided. The minimum separation distance represents a key limiting factor in productivity at a growing number of airports, with ripple effects on the entire air traffic system. The problem of vortex encounters is exacerbated with the advent of very large transports requiring increased separation and offsetting some of the economic advantages of the larger vehicles. Operating by current standards presents a bleak prospect for the future of air traffic. Consequently, there exists a keen practical interest in developing techniques for wake flow control and alleviation.

Prior attempts to control airplane trailing wakes can be grouped in two categories. One set seeks to alter the vortex structure, and the other group targets vortex instabilities that lead to vortex disintegration. An early technique for breakup of wake vortex was investigated by Crow and Bate [21], whereby airplane control surfaces were used to periodically alter the wing loading to introduce perturbations into the vortex system that ultimately lead to vortex instability. Crouch and Spalart [22] extended this method to airplanes with flap deployed, where quicker vortex breakup was accomplished by periodic movement of control surfaces to trigger instabilities associated with multiple trailing vortices. An undesirable by-product of this mode of control surface movement is the continual change in wing load, with implications on dynamic loads, airplane controllability, and ride quality. Recently, Greenblatt [23] demonstrated the feasibility of near-field vortex management via control of flow separation using pulse zero-net-mass-flux actuation on wing flaps.

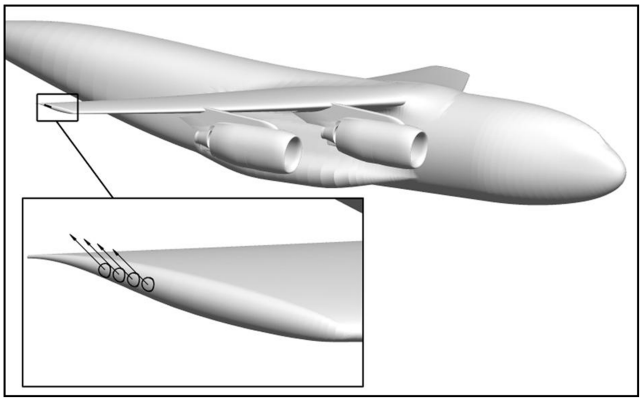

Fig. 15 System for the control of wing vortex.

A. Method of Vortex Control

The current study explores a technique based on fluidic actuation for control of tip vortex, as proposed in [24,25]. The flow actuation introduces time-varying perturbations into vortex elements to hasten vortex breakup. The control devices can be installed at the tips of lifting surfaces, including wing tips and edges of flap elements. The current approach can be used for the control of either airplane wing wakes or rotorcraft blade wakes, since it does not require usage of control surfaces. A schematic layout of the wake alleviation system for a typical transport is depicted in Fig. 15, which shows the flow control actuator at the tip of the wing. The system uses high-pressure bleed air from the engine compressor (or from other air sources), which is supplied to valves located close to the tips of the wing and/or the flap elements. Individual valves are connected to respective movable nozzles that control the fluid ejection. During actuation the jet from each of the individual nozzles is blown in the general lateral direction. The continuous jet is discharged through a nozzle that swivels intermittently at given frequency and within predefined azimuth bounds.

The controlled motion of each nozzle is prescribed to achieve maximum effect on vortex formation and its subsequent development. Various scanning patterns can be obtained by using select combinations of sinusoidal horizontal and vertical motions (i.e., sets of amplitude, frequency, and phase of the planar motions). Depending upon the frequency, the flow control can be effective in either accelerating vortex decay or in introducing instabilities leading to vortex disintegration.

B. Simulations of Trailing Wakes

The numerical method is validated with experimental data obtained in the Boeing vertical short-takeoff-and-landing wind tunnel for a rotorcraft blade. The blade was cantilevered to the wall for the purpose of measuring the blade tip-vortex strength, size, and position. The blade model was segmented in the span direction to effectively produce variations in spanwise twist. Although the blade was not rotating, this setup was used to control twist distribution to generate an aerodynamic blade loading similar to that of a rotorcraft in hover. Measurements of velocity were made at several cross

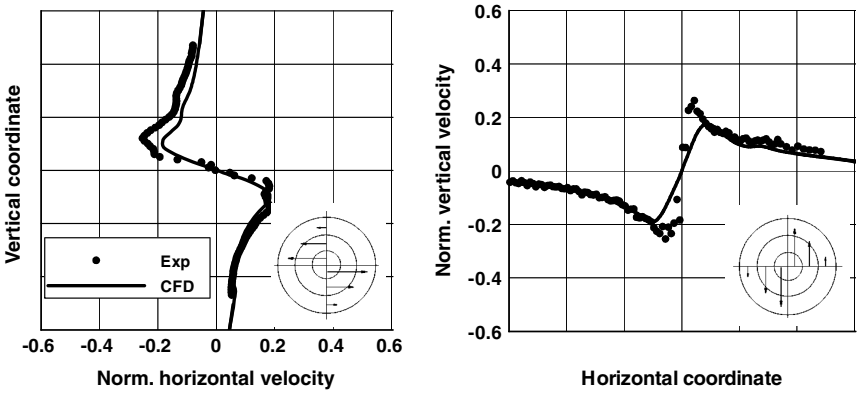

Fig. 16 Velocity profiles across the vortex at the 17.8 chord station.

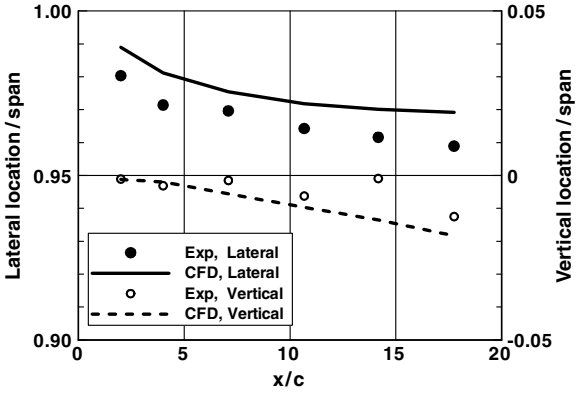

Fig. 17 Vortex position as a function of downstream distance.

sections downstream of the tip of the blade with the quantitative wake survey system. Free-air conditions using the SA turbulent model are used in the simulation, and the numerical model represents the blade mounted to an inviscid wall.

The current method addresses the flow development in the immediate rollup and the intermediate wake regions. A grid adaptation technique for vortex tracking is employed to ensure tight resolution around the vortex element [26]. The adaptation process will be reviewed in the context of flow control in the following section. The SA turbulence model was used. A Mach number of 0.15, Reynolds number of 1.25×10^6 based on blade chord length, and angle of attack of 6.5° were used for validation. The blade's computed lift coefficient was 0.55, consistent with the experimental measurement.

The ability of the simulation technique to capture the flow characteristics of the vortex is shown in Figs. 16 and 17. Figure 16 shows the horizontal and vertical velocity components normalized by the freestream velocity as functions of distance from the vortex center at a section downstream of the blade tip. The agreement is reasonable, but discrepancies exist. It is noted that the peak-to-peak velocity is underpredicted by nearly a constant amount at several cross-sectional stations along the wake. This implies that the vortex-tracking method adequately maintains the vortex strength. This systemic discrepancy is also attributed to the free-air simulation, whereby tunnel wall effects are not accounted for. The distance between peaks is also reasonably captured, though the simulated vortex tends to disperse more, relative to the experiment data. A comparison of the computed vortex location with experimental data is shown in Fig. 17. The lateral (spanwise) and vertical locations of the vortex center are scaled by the blade span. Here too, the

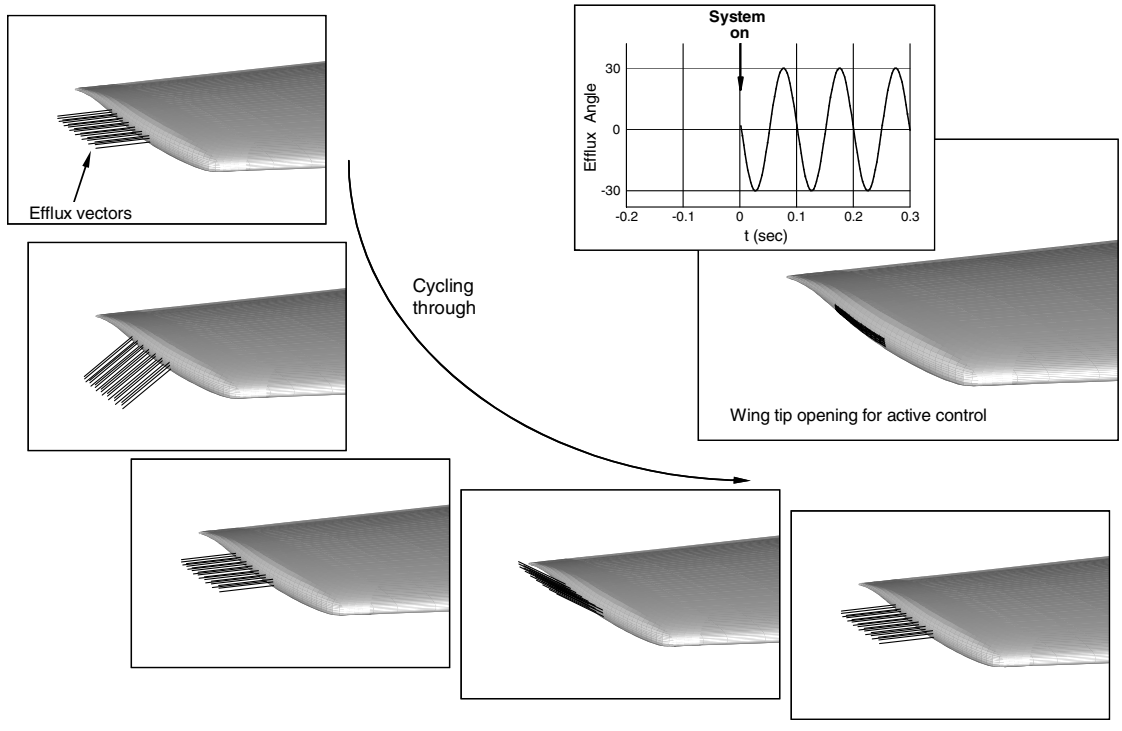

Fig. 18 Jet efflux pattern of the flow control system.

agreement is adequate, considering that the wind-tunnel walls are not represented in the simulation. Depending on the distances to the respective wind-tunnel walls, the effect of the walls is to push the tip vortex inboard and upward. The maximum tangential velocity of the wake is consistent with the experimental data of Ciffone and Orloff [27] obtained for a rectangular wing in a water tank. Further details of the validation study are described in [26].

C. Flow Control Simulations

The method for controlling wing tip-vortex development has been evaluated for a wing mounted on a vertical wall. No high-lift devices are included in the current analysis. The wing is defined by a set of supercritical airfoil sections. The planform has a semispan of 811 in., an aspect ratio of 6.6, and a taper ratio of 0.29. It consists of straight leading and trailing edges, with leading-edge sweep of 29°. A freestream Mach number of 0.25, angle of attack of 8°, and Reynolds number of 38.5×10^6 (based on C_{mac}) are used to represent final approach conditions. These conditions result in a lift coefficient of 0.68.

Special considerations must be given to grid resolution to ensure adequate representation of wing wake development, particularly in the context of active flow control. Proper modeling of the bounded wing viscous layers, vortex rollup, and downstream flow development is ensured only if the level of numerical dissipation is small in comparison with the viscous terms. Excessive numerical dissipation results in unrealistic vortex decay and therefore demands high grid resolution. Moreover, the diameter of the vortical element is quite small and it occupies a small portion of the computational domain. Clearly, without a priori knowledge of vortex location, a conventional grid system with adequate fineness presents an unacceptable option, since it is both wasteful and impractical. Therefore, the current study employs a grid adaptation technique for efficient modeling of high-resolution vortex flows [26,28].

The adaptation process is performed for the baseline flow (without flow control) by tracking the location of the minimum total pressure. When convergence is reached and grid adaptation is complete, the vortex core is usually represented by stencils of about 16×16 grid points on each of the cross-sectional grid surfaces. This procedure ensures that the rollup is well captured and the vortex core is preserved. The adapted grid obtained from the baseline flowfield is used for flow control computations. The vortex fitted grid occupies a sufficiently large volume such that the excursions of vortex core due to flow actuation are contained within this grid block.

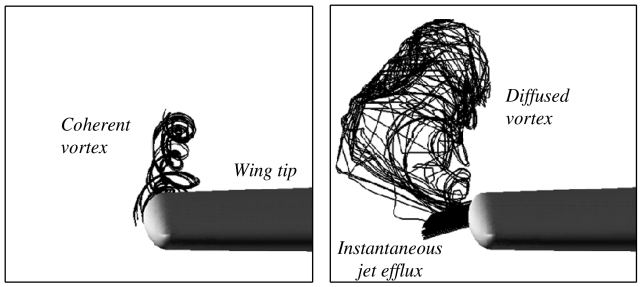

Fig. 19 Near-field wing-tip flow structure before and after actuation (front view).

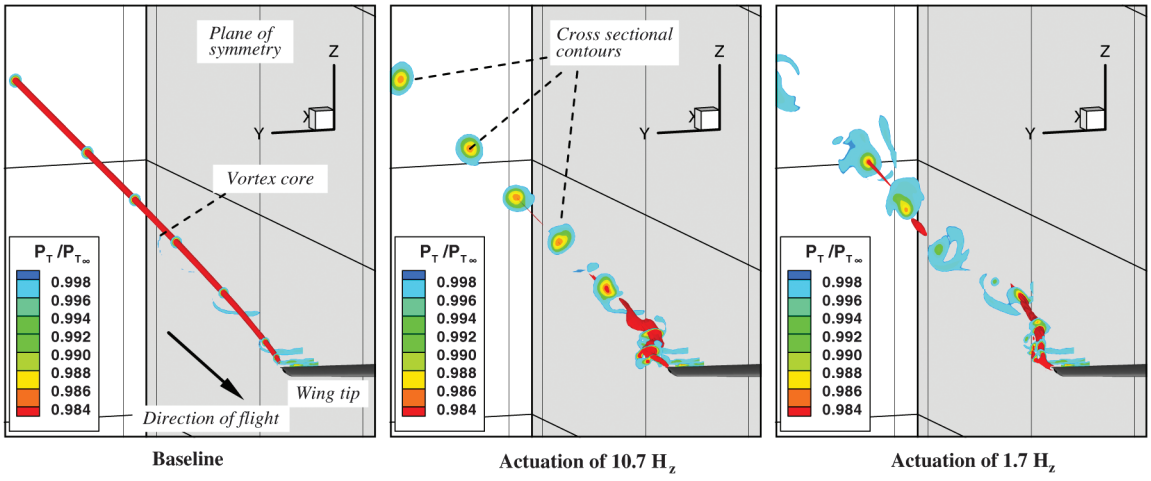

Fig. 20 Trailing vortex before and after application of flow control.

Actuation is applied at the edge of the wing tip. The boundary condition for the actuation is prescribed on the surface of the wing-tip cap. The exit plane of the ejection nozzle is defined by an elongated rectangular shape. The constant-mass-flow condition described in Sec. II is used with a Mach number of 0.64 when the jet is in the horizontal position. In the following simulations the actuation nozzle effectively moves up and down in the lateral direction in the range of $\pm 30°$ off the horizontal plane. This scanning pattern is schematically described in Fig. 18. The inset in the upper right shows the exit plane of the nozzle that extends from midchord to about 75% wing-tip chord station. The actuation is governed by a sinusoidal motion of the ejection nozzle. The actuation mechanism is also depicted in Fig. 18, where efflux vectors at phase intervals of $\pi/2$ are shown during one actuation cycle, starting with the downstroke from the horizontal position.

Results obtained for actuation frequencies of 10.7 and 1.07 Hz are presented here. To ensure similar temporal flow description, 2400 time steps per cycle are used for the high-frequency case, and 24,000 time steps per cycle are used for the low-frequency actuation.

Actuation at a frequency of 10.7 Hz is first considered for describing the flow excitation in the very near field. Figure 19 shows the flow structure in the front views, where the vortex is represented by the streakline traces off the wing tip during the time interval of one actuation cycle (0.093 s). A distinct vortex originates at the wing tip before active control is applied. The resulting flow after jet activation demonstrates that the intermittent mixing provided by the periodic motion of the jet perturbs the flow in the tip region and alters the development of the trailing vortex by reducing its strength and diffusing it in the cross plane.

The flowfields obtained with the two actuation frequencies are described next. The wake structures for the baseline and the controlled flows are depicted in Fig. 20, where the tip vortex is tracked by the total-pressure loss and the crossflow velocity. The vortex core is represented by isosurfaces of the respective flow properties. Cross-sectional contours are also shown at select streamwise stations. The computed baseline flow indicates that after the initial rollup phase, the vortex is asymptotically preserved, producing a coherent wake with a strong tip vortex. The trailing-wake flows due to active control are represented by flowfield snapshots of the respective actuation frequencies. In the high-frequency case the strength of the vortex is significantly reduced and the flow is nearly constant, with very small variations in wake structure. The interaction between the oscillatory jet and the crossflow is virtually invariant on the global time scale, and therefore the global impact on the wake structure is effectively decoupled from the operating frequency. On the other hand, the low-frequency oscillating jet introduces periodic disturbances along the tip vortex that propagate downstream. Here, remnants of the vortex core are represented by blobs defined by the respective flow properties. The motion of these fragmented vortical elements resembles a corkscrew pattern, formed by a combination of a wobbling motion in the cross plane and streamwise advance. Contrasted with the natural instabilities that evolve slowly, the current technique introduces perturbations in the region where the vortex originates, potentially triggering instabilities much sooner.

Additional diagnostics of flow development along the vortex core relative to the baseline case are shown in Fig. 21 for the high-frequency actuation. Flow properties at a sequence of time intervals of 0.093 s (corresponding to the duration of one actuation cycle) from the instant of jet activation are shown along the vortex core. Also, the characteristics along a vertical line that passes through the vortex core at the $x = 2850$ in. station are shown in the lower plots. The undisturbed vortex is described by the thick solid curves ($t = t0$). The other curves represent the impact of the control mechanism on vortex characteristics at progressive time intervals with the signal traveling downstream (in the positive x direction). The front of the perturbation wave corresponds to the last snapshot in the time sequence ($t6$), and it is represented by the dashed curve. The dashed line describes the state of the vortex at 0.558 s from the start of jet actuation. The high-frequency actuation is very effective at reducing vortex strength, as measured by the total-pressure loss and the crossflow velocity (represented by the tangential component of the velocity).

The effect of the lower jet frequency of 1.07 Hz on the trailing-wake flow is evaluated in Fig. 22. The perturbation waves along the vortex filament are shown at the same time intervals as in the high-frequency case. Periodically, the total-pressure loss is reduced to less than 0.5%, which translates to about 85% reduction in the original vortex strength. The maximum tangential velocity is periodically reduced to about 50% of the original undisturbed vortex. Similarly, the maximum vorticity (not shown) is being reduced by about two-thirds. In practical terms, considering the substantial reduction in

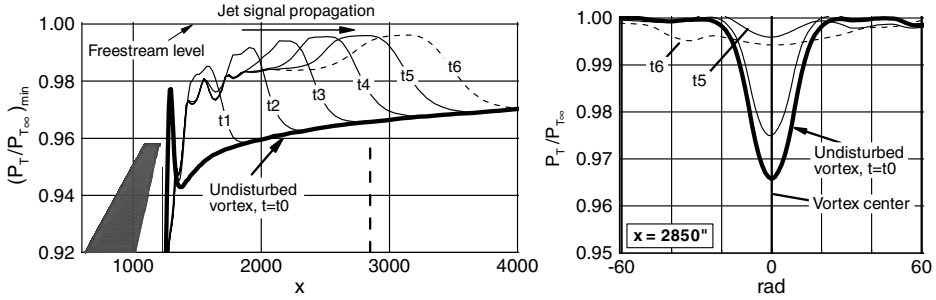

a) Total pressure

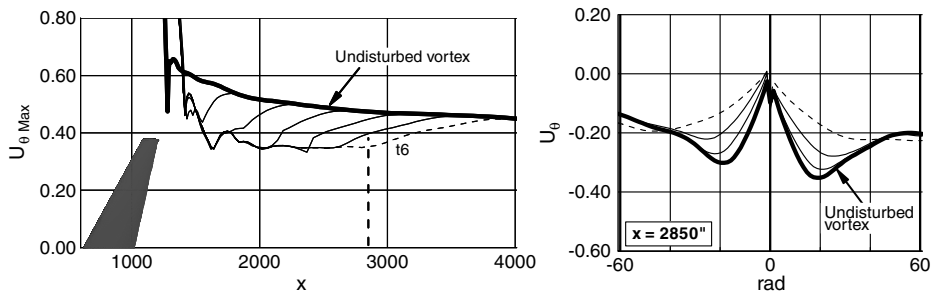

b) Crossflow velocity

Fig. 21 Instantaneous wake characteristics along vortex core and vertical wake profiles: high-frequency response.

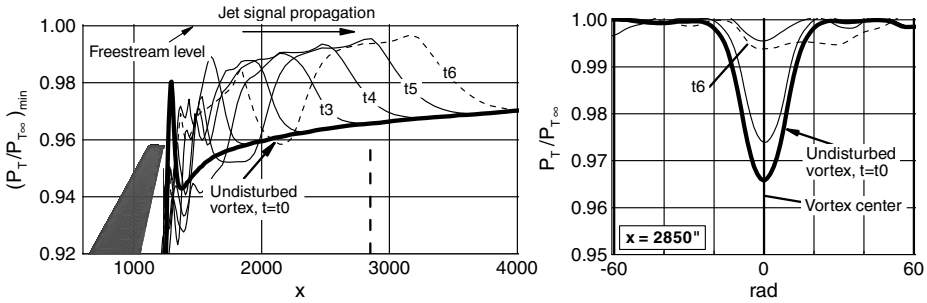

a) Total pressure

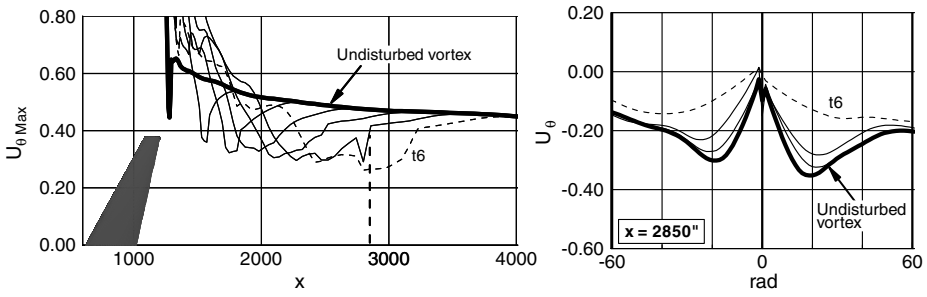

b) Crossflow velocity

Fig. 22 Instantaneous wake characteristics along vortex core and vertical wake profiles: low-frequency response.

crossflow realized by using active control, a following aircraft will experience a bumpy flight, but it will not be subject to a hazardous rolling motion.

The actuation at the edge of lifting surfaces affects the load distribution in the vicinity of the tip. Figure 23 shows wing lift oscillations over the respective actuation periods during the limit cycles. Families of instantaneous wing-load distributions are also presented for the respective actuation frequencies. The flow control produces very mild periodic variations of wing load in the outboard 15% segment of the wing span. The time-averaged lift is about 0.7% higher than the lift of the baseline wing, with only 0.17 and 0.44% lift oscillations for the high and low frequencies, respectively. Relative to active methods that use control surfaces for wake alleviation through wing-load management, the current technique has important advantages with respect to dynamic loads, flight control, and ride quality.

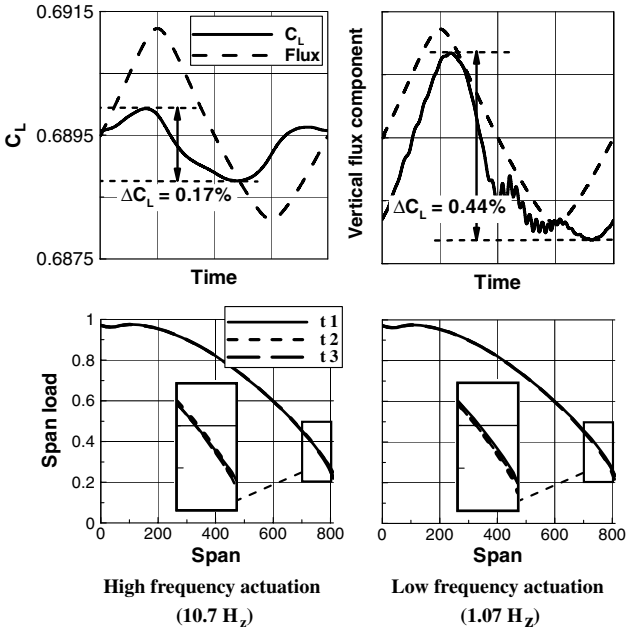

Fig. 23 Lift response and instantaneous wing-load distributions due to actuation.

VI. Conclusions

AFC techniques have been computationally examined for a diverse set of practical aerodynamic problems. Flow control modes based on intermittent jet pulsation and on sprinkler jet motion were employed. Pulsed-jet actuation is used to model either zero-mass-flux devices or actuators that require fluidic sources (i.e., engine bleed).

AFC for high-lift systems can potentially lead to performance enhancement over the practical range of angles of attack. Substantial lift increment can be realized by exploiting synergistic effects using actuation at individual wing elements. Depending on the flow conditions, the full benefit of nonlinear augmentation is realized when the actuation is simultaneously applied at select ports, producing lift levels approaching the inviscid limit. This has very important ramifications, since there are high payoffs for vehicles that can operate from very short fields, from both economical and operational standpoints.

In the engine vortex problem associated with ground operation, the pulsed jets and the sprinkler systems have resulted in the reduction of vortex ingestion and its concomitants, the risks of FOD and engine surge. Wide-area coverage of actuation is a key attribute that makes the sprinkler system especially attractive for control of unsteady vortices.

The sprinkler jet has also been used for control of trailing wakes, whereby flow actuation introduces time-varying perturbations into wing vortex elements to hasten vortex breakup. Depending upon the frequency of actuation, this actuation effectively disrupts the wake flow by either accelerating vortex decay or by encouraging instabilities along the vortex element. This effectively renders milder wakes and more benign conditions for following airplanes. High-frequency actuation results in significantly lower blade-to-blade vortex interactions in rotorcraft applications, with implications to reduced noise.

Although the set of results from numerical simulations are very encouraging, we recognize that practical implementations of the flow control concepts require thorough system integration analyses. The range of optional implementations offered by AFC implies that a pragmatic approach to a practical design that encompasses

other disciplines such as structures, noise, and power systems is indispensable.

References

[1] Sellers, W. L., III, Jones, G. S., and Moore, M. D., "Flow Control at NASA Langley in Support of High-Lift Augmentation," AIAA Paper 2002-6006, 2002.

[2] Wygnanski, I., "The Variables Affecting the Control of Separation by Periodic Excitation," AIAA Paper 2004-2505, 2004.

[3] Tilmann, C. P., Kimmel, R. L., Addington, G. A., and Myatt, J. H., "Flow Control Research and Applications at the AFRL's Air Vehicles Directorate," AIAA Paper 2004-2622, 2004.

[4] Anders, S. G., Sellers, W. L., III, and Washburn, A. E., "Active Flow Control Activities at NASA Langley," AIAA Paper 2004-2623, 2004.

[5] Kibens, V., and Bower, W. W., "An Overview of Active Flow Control Applications at the Boeing Company," AIAA Paper 2004-2624, 2004.

[6] Buning, P. G., Chui, I. T., Obayashi, S., Rizk, Y. M., and Steger, J. L., "Numerical Simulation of the Integrated Space Shuttle Vehicle in Ascent," AIAA Paper 1988-435, 1988.

[7] Shmilovich, A., and Yadlin, Y., "Engine Vortex Flows and Methods of Ground Vortex Alleviation," *Proceedings of the 3rd International Conference on Vortex Flows and Vortex Models*, Yokohama, Japan, 2005.

[8] Shmilovich, A., and Yadlin, Y., "Engine Ground Vortex Control," AIAA Paper 2006-3006, 2006.

[9] Shmilovich, A., and Yadlin, Y., "Flow Control for the Systematic Buildup of High Lift Systems," *Journal of Aircraft*, Vol. 45, No. 5, Sept.–Oct. 2008, pp. 1680–1688.
doi:10.2514/1.35327

[10] Khodadoust, A., and Shmilovich, A., "High Reynolds Number Simulations of Distributed Active Flow Control for a High-Lift System," AIAA Paper 2007-4423, 2007.

[11] Kiedaisch, J., Demanett, B., and Nagib, H., "Active Flow Control Applied to High-Lift Airfoils Utilizing Simple Flaps," AIAA Paper 2006-2856, 2006.

[12] Ying, S. X., Spaid, F. W., McGinley, C. B., and Rumsey, C. L., "Investigation of Confluent Boundary Layers in High-Lift Flows," AIAA Paper 1998-2622, 1998.

[13] Strong, J. C., "Operating Report for the Wind Tunnel Test of the Two-Dimensional Supercritical High Lift Development Model LB-437A in the McAir Low Speed Wind Tunnel," McDonnell Douglas, Rept. MDC J6856, 1975.

[14] Shmilovich, A., and Yadlin, Y., "Active Flow Control for Practical High-Lift Systems," *Journal of Aircraft*, Vol. 46, No. 4, 2009, pp. 1354–1364.
doi:10.2514/1.41236

[15] Johns, C. J., "The Aircraft Engine Inlet Vortex Problem," AIAA Paper 2002-5894, 2002.

[16] Smith, D. M., and Dorris, J., "Aircraft Engine Apparatus with Reduced Inlet Vortex," U.S. Patent 6,129,309, 2002.

[17] Shmilovich, A., Yadlin, Y., Smith, D. M., and Clark, R. W., "Active System for Wide Area Suppression of Engine Vortex," U.S. Patent 6,763,651, 2004.

[18] Funk, R., Parekh, D., Smith, D. M., and Dorris, J., "Inlet Vortex Alleviation," AIAA Paper 2001-2449, 2001.

[19] Yadlin, Y., and Shmilovich, A., "Simulation of Vortex Flows for Airplanes in Ground Operations," AIAA Paper 2006-0056, 2006.

[20] Crow, S. C., "Stability Theory for a Pair of Trailing Vortices," *AIAA Journal*, Vol. 8, No. 12, Dec. 1970, pp. 2172–2179.
doi:10.2514/3.6083

[21] Crow, S. C., and Bate, E. R., "Lifespan of Trailing Vortices in a Turbulent Atmosphere," *Journal of Aircraft*, Vol. 13, No. 7, 1976, pp. 476–482.
doi:10.2514/3.44537

[22] Crouch, J. D., and Spalart, P. R., "Active-Control System for Breakup of Airplane Trailing Vortices," *AIAA Journal*, Vol. 39, No. 12, Dec. 2001, pp. 2374–2381.
doi:10.2514/2.1244

[23] Greenblatt, D., "Management of Vortices Trailing Flapped Wings via Separation Control," AIAA Paper 2005-0061, 2005.

[24] Shmilovich, A., Yadlin, Y., Clark, R. W., and Leopold, D., "Apparatus and Method for the Control of Trailing Wake Flows," U.S. Patent 7,100,875, 2006.

[25] Shmilovich, A., Yadlin, Y., Clark, R. W., and Leopold, D., "Apparatus and Method for the Control of Trailing Wake Flows," U.S. Patent 7,597,289, 2009.

[26] Yadlin, Y., Shmilovich, A., and Narducci, R., "A Method and Applications for Tracking Airplane Trailing Wakes," AIAA Paper 2010-0324, 2010.

[27] Ciffone, D. L., and Orloff, K. L., "Far-Field Wake-Vortex Characteristics of Wings," *Journal of Aircraft*, Vol. 12, No. 5, 1975, pp. 464–470.
doi:10.2514/3.59825

[28] Shmilovich, A., and Yadlin, Y., "Flow Control of Airplane Trailing Wakes," *Proceedings of the 4th International Conference on Vortex Flows and Vortex Models*, Daejeon, Korea, 2008.

E. Livne
Associate Editor